Carcinogenesis, 2015, Vol. 36, No. 9, 1008–1018

doi:10.1093/carcin/bgv081
Advance Access publication June 7, 2015
Original Manuscript

ORIGINAL MANUSCRIPT

Hepatocellular carcinoma-derived exosomes promote motility of immortalized hepatocyte through transfer of oncogenic proteins and RNAs

Mian He[1,†], Hao Qin[2,†], Terence C.W.Poon[3,†], Siu-Ching Sze[1], Xiaofan Ding[1], Ngai Na Co[1], Sai-Ming Ngai[2], Ting-Fung Chan[2] and Nathalie Wong[1,4,*]

[1]Department of Anatomical and Cellular Pathology and [2]School of Life Sciences, The Chinese University of Hong Kong, Shatin, Hong Kong, China, [3]Pilot Laboratory and Proteomics Core, Faculty of Health Sciences, University of Macau, Avenida da Universidade, Taipa, Macau, China and [4]State Key Laboratory in Oncology in South China, The Chinese University of Hong Kong, Shatin, Hong Kong, China

*To whom correspondence should be addressed. Tel: +852 2632 1128; Fax: +852 2637 6274; Email: natwong@cuhk.eud.hk

†These authors contributed equally to this work

Abstract

Exosomes are increasingly recognized as important mediators of cell–cell communication in cancer progression through the horizontal transfer of RNAs and proteins to neighboring or distant cells. Hepatocellular carcinoma (HCC) is a highly malignant cancer, whose metastasis is largely influenced by the tumor microenvironment. The possible role of exosomes in the interactions between HCC tumor cell and its surrounding hepatic milieu are however largely unknown. In this study, we comprehensively characterized the exosomal RNA and proteome contents derived from three HCC cell lines (HKCI-C3, HKCI-8 and MHCC97L) and an immortalized hepatocyte line (MIHA) using Ion Torrent sequencing and mass spectrometry, respectively. RNA deep sequencing and proteomic analysis revealed exosomes derived from metastatic HCC cell lines carried a large number of protumorigenic RNAs and proteins, such as MET protooncogene, S100 family members and the caveolins. Of interest, we found that exosomes from motile HCC cell lines could significantly enhance the migratory and invasive abilities of non-motile MIHA cell. We further demonstrated that uptake of these shuttled molecules could trigger PI3K/AKT and MAPK signaling pathways in MIHA with increased secretion of active MMP-2 and MMP-9. Our study showed for the first time that HCC-derived exosomes could mobilize normal hepatocyte, which may have implication in facilitating the protrusive activity of HCC cells through liver parenchyma during the process of metastasis.

Introduction

Hepatocellular carcinoma (HCC) is a primary malignancy of hepatocyte that is rapidly fatal. Although diagnostic methods and therapeutic strategies for HCC have been improved in last decades, long-term survival of HCC patients still remains poor due to high metastases and/or postsurgical recurrence rate (1). Whether tumor will undergo local or distant metastasis is determined by both the metastatic potential of tumor cell itself and the signals from its microenvironment (2). Multiple signaling pathways and genes are involved in the crosstalk between the HCC tumor cells and their microenvironment (3). Of interest, HCC metastatic propensity may also be affected by tumor-surrounding tissue milieu. Elevated expression of macrophage colony-stimulating factor in hepatocytes of non-cancerous surrounding hepatic parenchyma can create an anti-inflammatory microenvironment by mediating the Th1/Th2-like cytokine shift, which may promote HCC progression and venous metastases (4). Besides, tumor-activated hepatocytes are able to change the transcriptional profiles of colon cancer cells to support their

Received: December 17, 2014; **Revised:** April 30, 2015; **Accepted:** May 20, 2015

Abbreviations

cDNA	complementary DNA
DMEM	Dulbecco's modified Eagle's medium
FBS	fetal bovine serum
GO	gene ontology
HCC	hepatocellular carcinoma
MMP	matrix metalloproteinase
ncRNA	non-coding RNA
PBS	phosphate-buffered saline

hepatic metastasis (5). Despite hepatocyte cells are believed to be involved in the metastatic process of HCC, interactions between hepatoma cells and adjacent hepatocytes have not received much attention so far.

Exosomes are tiny membrane vesicles that are released into the exterior following the fusion of multivesicular endosomes with plasma membrane by many different cell types, including cancer cells (6). Growing evidences indicate exosomes can modulate intercellular communication and tumor progression through the horizontal transfer of RNAs and proteins to neighboring or distant cells (6–8). Nonetheless, the function of exosome depends on the cell type of origin as well as its content. It is recognized that exosomes play key roles in tumor metastasis through mediating complex interaction between tumor cells and microenvironment (9,10). Since exosomes are the carriers of multiple RNA and protein molecules, RNA deep sequencing and proteomic profiling are promising platforms to explore global profiles of exosomal components, which will aid understandings of their biologic functions.

In this study, we comprehensively characterized the transcriptome and proteome of exosomes derived from HCC cell lines by Ion Torrent sequencing and mass spectrometry, respectively. Of interest, we found exosomes from highly metastatic HCC cell lines could markedly induce migratory and invasive behaviors of non-motile hepatocytes. The internalization of exosomes could activate PI3K/AKT and MAPK signaling pathway, and increased secretion of matrix metalloproteinases (MMP)-2 and MMP-9 that favored cell invasion. This phenomenon may have inference on a novel interplay between HCC tumor cells and liver parenchyma cells, where cancer-derived exosomes might alter the liver milieu in support of tumor metastasis.

Materials and methods

Cell lines and cell culture

The inhoused established human HCC cell lines HKCI-C3 and HKCI-8 were maintained in RPMI 1640 medium supplemented with 10% fetal bovine serum (FBS) and 1× Insulin–Transferrin–Selenium–Sodium Pyruvate (ITS-A) (Life Technologies) as described previously (11). HCC cell line MHCC97L and immortalized hepatocyte cell line MIHA were propagated in Dulbecco's modified Eagle's medium (DMEM) complete medium. All cell lines were routinely authenticated, including STR genotyping and mycoplasma detection.

Exosome purification

Exosomes were isolated from the cell culture supernatant by differential centrifugations as described previously (8,12), with some modification. In brief, 2.5 × 10^6 HCC cells were seeded in 150 mm dish and allowed to recover for 24 h. Then cells were washed twice with prewarmed phosphate-buffered saline (PBS) and culture medium was replaced with exosome-free medium supplemented with 10% exosomes-depleted FBS. To minimize copurification of exosomes from FBS, exosomes-depleted FBS was prepared by overnight ultracentrifugation before utilized in the preparation of complete medium. After 2 days of culture, conditioned medium from cells reaching ~90% confluence was harvested and subjected to serial centrifugations for 10 min at 500*g* and 30 min at 16 500*g*, followed by filtration through a 0.22-μm pore filter (Millipore). The filtrated medium was ultracentrifuged at 110 000*g* for 70 min to harvest exosomes. Exosome pellet was washed with PBS and then collected by ultracentrifugation at 110 000*g* for 70 min on a 40% w/v sucrose cushion. The floating exosomes were collected and pelleted again by ultracentrifugation at 110 000*g* for 70 min. Recovered exosomes were measured for their protein amount using Bradford protein assay (Bio-Rad)

Size distribution analysis by qNano

Scanning ion occlusion sensing analysis was performed using the qNano instrument (Izon, Christchurch, New Zealand). The operation of qNano was strictly according to manufacturer's instructions. Isolated exosome samples were resuspended in PBS and cleared by passing through a 0.22 μm filter. All samples were measured under 44.5 mm stretch and 0.64V voltage using NP100 membranes. Samples were calibrated by CPC100 standard particles diluted 1000-fold under identical settings.

Western blot analysis

Fifteen microgram exosomal protein or total cellular lysates were resolved on 10% SDS-PAGE and electrophoretically transferred onto nitrocellulose membranes. Specific primary antibodies used included Alix (Cell Signaling), TSG101 (Santa Cruz), HSC70 (Enzo Life Sciences), Grp94 (Enzo Life Sciences), S100A4 (Abcam), CAV1 (Abcam), CAV2 (Cell Signaling), MET (Cell Signaling), p-MET (Tyr1234/1235) (Cell Signaling), total AKT (Cell Signaling), p-AKT (Ser473) (Cell Signaling), total MEK1/2 (Cell Signaling), p-MEK1/2 (Ser217/221) (Cell Signaling) and GAPDH (Millipore). After incubation with horseradish peroxidase-conjugated secondary antibodies, protein bands were visualized using enhanced Enhanced chemiluminescence (GE Healthcare).

Ion torrent sequencing

RNA-Seq library preparation was performed with ion torrent RNA-Seq Kit v2 (Life Technologies) following the manufacturer's protocol (Publication Part Number 4476286 Rev. B). Briefly, 50 ng total exosomal RNA was fragmented to about 100–200 nt by RNase III. Ion Adaptors were ligated to the both ends of fragmented RNA, which later were reverse transcribed to complementary DNA (cDNA) and PCR-amplified for a total of 16 cycles. Emulsion PCR and enrichment steps were carried out using the Ion OneTouch 200 Template Kit v2 DL (Life Technologies) and associated protocol (Publication Number MAN0006957). In brief, the whole transcriptome library was added to the emulsion PCR master mix at a limiting dilution. The emulsion and amplification procedures were automatically run by the Ion OneTouch DL configuration (Life Technologies). Then, ion sphere particles were recovered and template-positive ion sphere particles were enriched by Dynabeads MyOne Streptavidin C1 Beads (Life Technologies). The Ion PGM 200 sequencing kit (Life Technologies) was used with the Personal Genome Machine (PGM) sequencer following the recommended protocol (Publication Number 4474246 Rev. D). Enriched ISPs were prepared for sequencing as described in the protocol and loaded onto the Ion 314 Chips. Each chip was sequenced for 125 cycles.

Mapping and expression calculation

Reads were mapped by TMAP 0.3.7 developed by Life Technologies for Ion Torrent sequencing against human genome hg19 obtained from UCSC genome browser. The peaks of mapped reads were individually identified by inhouse-developed pipelines, whose peak lengths were greater or equal to 10 nt and the expressions, defined as the numbers of mapped reads, were greater than 2. Then all peaks from each sample were merged to expression regions. The location identity of expression regions was determined by inhouse-developed pipelines using Refseq annotation from UCSC genome browser. The expression of a gene was calculated by averaging the expressions of all expression regions that were overlapped with the gene. The expressions were normalized by the number of reads mapped to ribosomal RNA genes.

Proteomics profiling by mass spectrometry

Thirty microgram exosomal proteins were resolved on 4–12% Bis–Tris Gels (Bio-Rad Laboratories) and visualized by Coomassie blue staining. The

identities of the protein spots in 1D SDS-PAGE were obtained by tandem mass spectrometry, as described previously (13). Briefly, gels were consecutively cut into 0.9 mm gel slices, distained and digested overnight with modified porcine trypsin (Promega). After cleaned up with C18 ZipTips (Millipore), tryptic peptides were subjected to tandem MS analysis using Ultraflex III MALDI-TOF/TOF mass spectrometry (Bruker Daltonics). The acquired tandem MS data were searched via the MASCOT search engine to obtain the protein identities by the peptide mass fingerprinting approach.

Gene clustering and GO enrichment

The expression of genes were rescaled by dividing the expression by the largest value among the samples. The clustering was performed by R package gplots 2.14.2. The Gene Ontology (GO) enrichment was performed by DAVID as described (14).

Migration and invasion assay

The cell migratory and invasive abilities were assessed by Transwell migration assay (Corning) and BioCoat Matrigel Invasion assay (BD Biosciences), respectively. For each assay, MIHA cells (5×10^4 for migration, 1×10^5 for invasion) in serum-free DMEM with or without 10 μg HCC cell lines-derived exosomes were seeded onto the upper chamber of the insert. After 48 h of incubation, the membrane of insert was fixed in 100% methanol and stained with hematoxylin. The number of migrated or invaded cells was scored for at least 10 microscope fields (×200). The mean value was expressed as a percentage relative to the control and represented three independent experiments run in duplicate.

RNA extraction, cDNA synthesis and quantitative RT-PCR

Total RNA from cell lines and exosomes were isolated by miRCURY RNA isolation kit (Exiqon) according to manufacturer's protocol. After quantitation by Bioanalyzer (Agilent Technologies), RNA was treated with RNase-free DNase I (Life Technologies) to eliminate genomic DNA carryover and then reverse transcribed to complementary DNA using Multiscribe reverse transcriptase (Life Technologies). First-strand cDNA was subjected to Taqman assay for target genes in Universal PCR Mix (ABI). The emission intensity was measured by iCycler IQ detection system, using fluorophore FAM490 or VIC530 (ABI). Because of lacking reference genes in exosomes, we used RNA quantitation for normalization to compare gene expression levels between exosomes and donor cells. Except this situation, gene expression was normalized against 18S rRNA.

Transfection

siRNAs specific to MET, CAV1 and CAV2 (Silencer Select siRNA s8702, s2448 and s2450) and a control siRNA (Silencer Select Negative Control No.1 siRNA) were purchased from Life Technologies. pCMV6-ENTRY-MET plasmid was acquired from OriGene Technologies. CAV1 and CAV2 plasmids were constructed in-house by subcloning PCR-amplified human CAV1 and CAV2 cDNA into pcDNA3.1 vector. All plasmids were sequence verified by Sanger. Transfection of plasmids or siRNAs was performed using Lipofectamin 2000 (Life Technologies). For siCAV1 and siCAV2 pretreated MIHA (Figure 5C), cell medium of transfected MIHA was replaced with fresh DMEM supplemented with 0.5% exosomes-depleted FBS in the presence or absence of MHCC97L-derived exosomes. For overexpression studies of MET and Caveolins, transfected MIHA cells were subjected to transwell migration and matrigel invasion assay after 24-h posttransfection. For knockdown experiments of MET and CAV1 in MHCC97L (Figure 5G), transfected cells were washed twice with pre-warmed PBS to remove Lipofectamine–siRNA complex. Thereafter, cell medium was replaced with exosome-free medium supplemented with 10% exosomes-depleted FBS and cultured for a further 48 h before exosomes isolation.

Gelatin zymography

MHCC97L exosomes-treated and -untreated MIHA cells were grown in serum-free DMEM for 48 h. Conditioned medium were collected and centrifuged to deplete floating cells and cell debris. After quantitation by Bradford protein assay (Bio-Rad), samples containing equal protein amounts were mixed with non-reducing 4× sample buffer, and run on a 8% polyacrylamide gels containing 0.1% gelatin. After electrophoresis, gels were renatured and subsequently incubated in developing buffer at 37°C for overnight. After incubation, gels were stained with 0.4% Coomassie Brilliant Blue R-250 for 1 h and then destained with an appropriate destaining solution. Areas of protease activity appeared as clear bands in the dark blue background where the protease had digested the substrate.

Statistical analysis

All values were presented as the mean ± SEM from three independent experiments. The effect of HCC-derived exosomes on MIHA migratory and invasive abilities were assessed by Student's *t*-test. Gene expressions in MIHA cells between the absence and the presence of MHCC97L-secreted exosomes treatment were also compared by Student's *t*-test. Values of $P < 0.05$ were considered to be statistically significant. All statistical analysis were performed using Graphpad Prism, version 6.05.

Results

Isolation of HCC-derived exosomes

HCC cell lines, HKCI-C3, MHCC97L and HKCI-8, and immortalized hepatocyte MIHA were study models for our exosomes investigations. Among them, MIHA and HKCI-C3 were non-motile cell lines, while MHCC97L and HKCI-8 showed high motile ability through transwell migration and matrigel invasion chambers (Figure 1A).

Exosomes were isolated from culture supernatant using standard differential centrifugations. Based on its properties, including its size (30–150nm) and density in sucrose (1.13–1.19 g/ml), we optimized the isolation protocol by adding two additional steps, which involved a 0.22-μm filtration and sucrose cushion ultracentrifugation, to eliminate contamination from other types of secreted vesicles (Figure 1B). qNano analysis revealed that isolated exosomes were ~118 nm in diameter (Figure 1C) and the number of exosomes did not differ much between the four cell lines examined (Figure 1D). However, quantitation of exosomal proteins showed exosomes from HCC cell lines carried higher amounts of protein content than exosomes from immortalized hepatocyte MIHA (Figure 1E). The purity of exosomes obtained from four cell lines was further confirmed by western blot which showed presence of exosome-specific markers TSG101, Alix and HSC70, and absence of endoplasmic reticulum marker Grp94 (Figure 1F).

Transcriptome analysis of HCC-derived exosomes

In line with published literature (7,8), we also found the nucleotide content of HCC-derived exosomes to be predominantly RNA species. In addition, we found exosomes harbor little or negligible ribosomal RNA (18S and 28S rRNA) when compared with their parental cells (Figure 2A). Notably, the major peak of exosomal RNA was between 500 and 4000bp, suggesting a variety of mRNAs or long non-coding RNAs (lncRNA) were confined within the exosomes. Some small RNA was also detected (Figure 2A).

To further determine the identities of these RNA molecules, we performed Ion Torrent sequencing technology to characterize the exosomal transcriptome. In four cell lines, over 95% of total reads were successfully mapped to the human reference genome (UCSC; hg19) (Supplementary Table 1, available at *Carcinogenesis* Online). Among the mapped reads, ~90% of reads were 5.8 rRNA sequences (Figure 2B). The remaining mapped reads belonged to mRNA of coding genes, known non-coding RNA, and some intergenic RNA fragments. Our analysis suggested exosomes from these four cell lines have a similar pattern of RNA distribution. We further analyzed the abundance of each RNA by normalizing against 5.8 rRNA, because it was the most abundant RNA specie in each cell line derived exosomes. In total, 1606 protein coding genes were detected with a normalized expression value of greater than 2 in one sample or

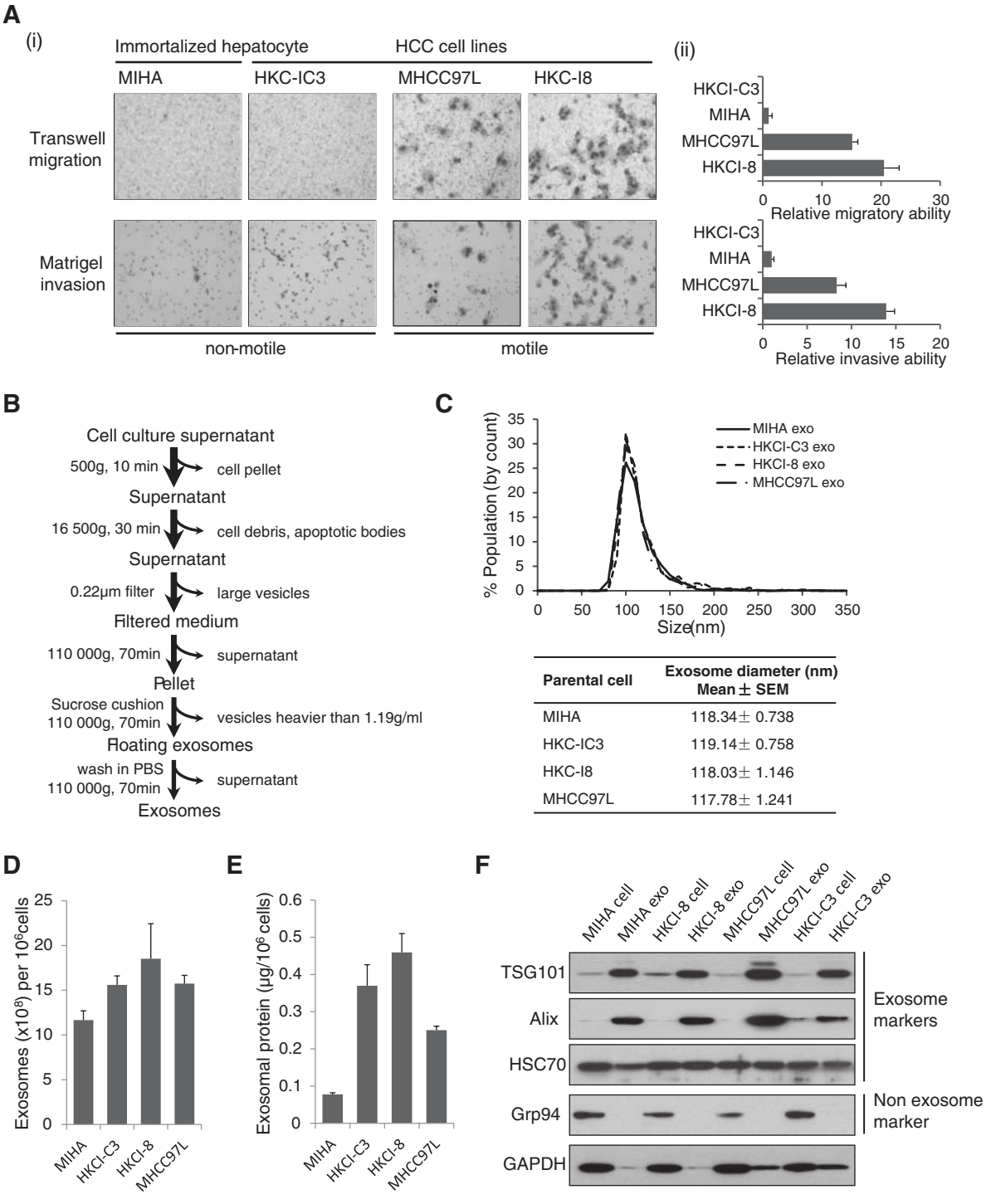

Parental cell	Exosome diameter (nm) Mean ± SEM
MIHA	118.34± 0.738
HKC-IC3	119.14± 0.758
HKC-I8	118.03± 1.146
MHCC97L	117.78± 1.241

Figure 1. Characterization of HCC-derived exosomes. (**A**) Migratory and invasive abilities of MIHA, HKCI-C3, MHCC97L and HKCI-8 were determined by migration and invasion assay. Original magnification ×200. (**B**) Strategy for exosomes purification from the cell culture supernatants based on differential centrifugations. (**C**) Size distribution analysis of purified exosomes by qNano instrument. (**D**) Number of total vesicles released by each cell line was estimated by qNano. (**E**) Measurement of total exosomal proteins per 1 million cells isolated from culture supernatant of four cell lines. (**F**) Equal amount of total protein from isolated exosomes and parental cell lysates were analyzed by immunoblotting analysis for TSG101, Alix, HSC70, Grp94 and GAPDH. Data shown represent mean ± SEM from three independent experiments.

more (Supplementary Table 2, available at *Carcinogenesis* Online). The top 10 enriched GO categories based on 692 HCC-specific exosomal coding genes have also been determined and highlighted in Supplementary Figure 1 is available at *Carcinogenesis* Online. Given the difference in the motile properties of parental cells, we found 121 coding genes to be differentially expressed in exosomes from motile and non-motile cell lines. Supervised clustering of selected genes was able to classify samples into non-motile and motile groups as well (Figure 2C left). Genes unique in motile HCC cell line-derived exosomes are listed (Figure 2C right). Moreover, several genes were specifically expressed in HCC-derived exosomes but absent in exosomes derived from MIHA (Figure 2D).

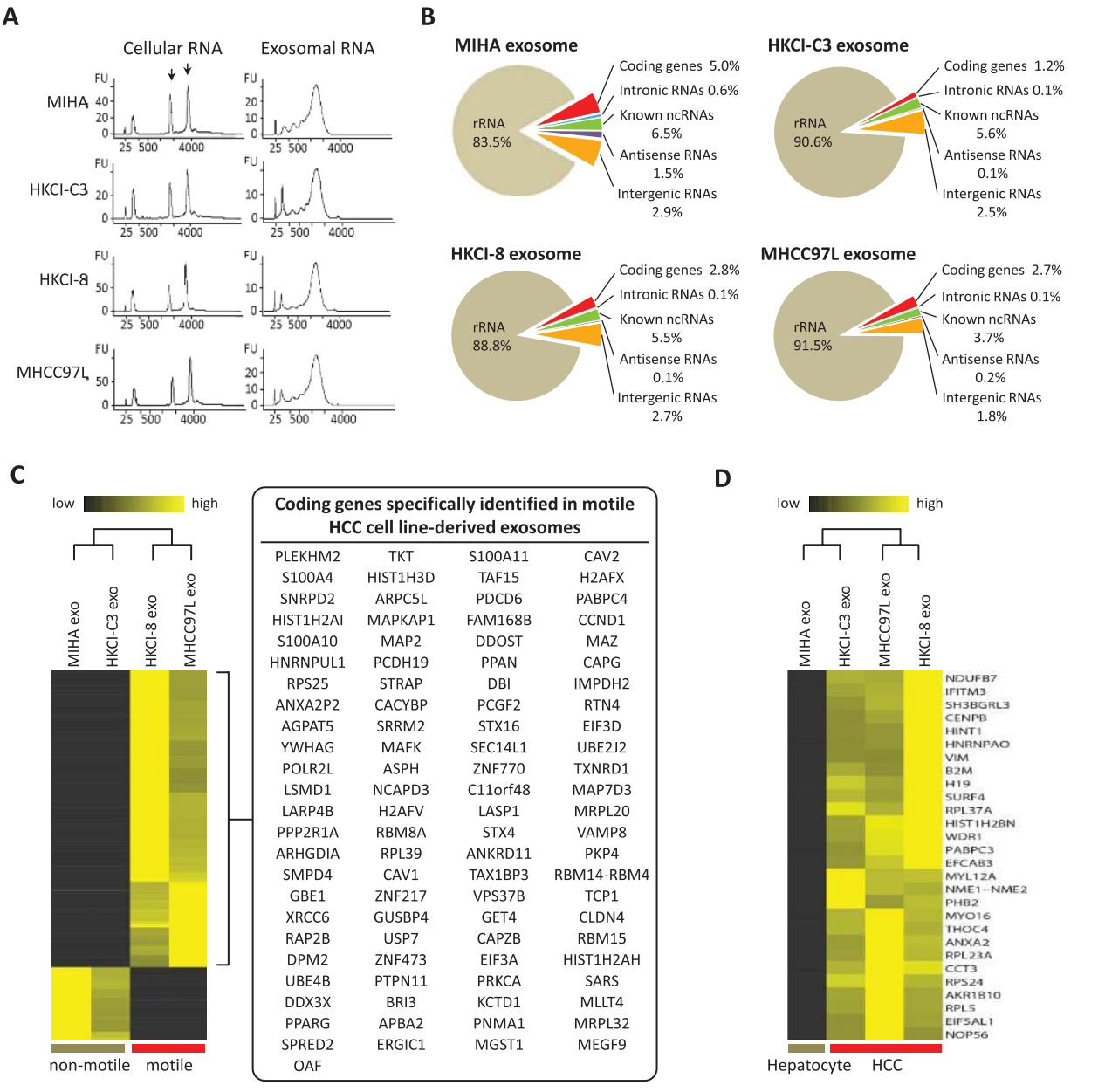

Figure 2. Transcriptome analysis of HCC-derived exosomes. (**A**) Bioanalyzer profiles of total cell RNA and exosomal RNA. Arrows indicate the 18S and 28S rRNA subunits present in cells. (**B**) Classification of mapped RNA-seq reads among transcriptome. (**C**) Supervised clustering using 121 differentially expressed coding genes classified the samples into two groups as well: non-motile and motile (left). Coding genes present in motile HCC cell line-derived exosomes were listed (right). (**D**) Supervised clustering of HCC specific exosomal genes.

Besides coding genes, a large variety of non-coding RNA species were also identified (Supplementary Table 3, available at *Carcinogenesis* Online). Among them, signal recognition particle RNA (SRP-RNA), Y-RNA, small nuclear ribonucleic acid (snRNA) and Vault RNA were abundantly present.

Mass spectrometry analysis for exosomal proteins

Differences among exosomal protein profiles could be observed in 1D-PAGE assay (Supplementary Figure 2, available at *Carcinogenesis* Online). Several protein bands (e.g. 20 kDa) were clearly enriched in metastatic HCC cells-derived exosomes. We further characterized the proteome profiles of HCC-derived exosomes using mass spectrometry and identified 277 proteins (Supplementary Table 4, available at *Carcinogenesis* Online). Comparing the exosomal proteome of each cell line, 213 proteins were only detected in HCC cell lines secreted exosomes, and 158 proteins were specifically expressed in exosomes from highly malignant HCC cells (Figure 3A). There were 25 proteins shared among all exosomes from four cell lines, the majority of which were exosomal markers and exosomes secreting-related proteins, such as structure proteins, heat shock proteins, syndecan-syntenin-ALIX, Ras-related proteins and vacuolar protein sorting-associated proteins (Figure 3B). Candidate proteins with known functions in carcinogenesis and metastasis, such as RRAS, CD44, CDC42 and CLND3, were identified in exosomes secreted from HCC or motile cell lines, respectively (Figure 3B). Quantification of exosomal proteins revealed some exosomal proteins to be differentially expressed in HCC cell

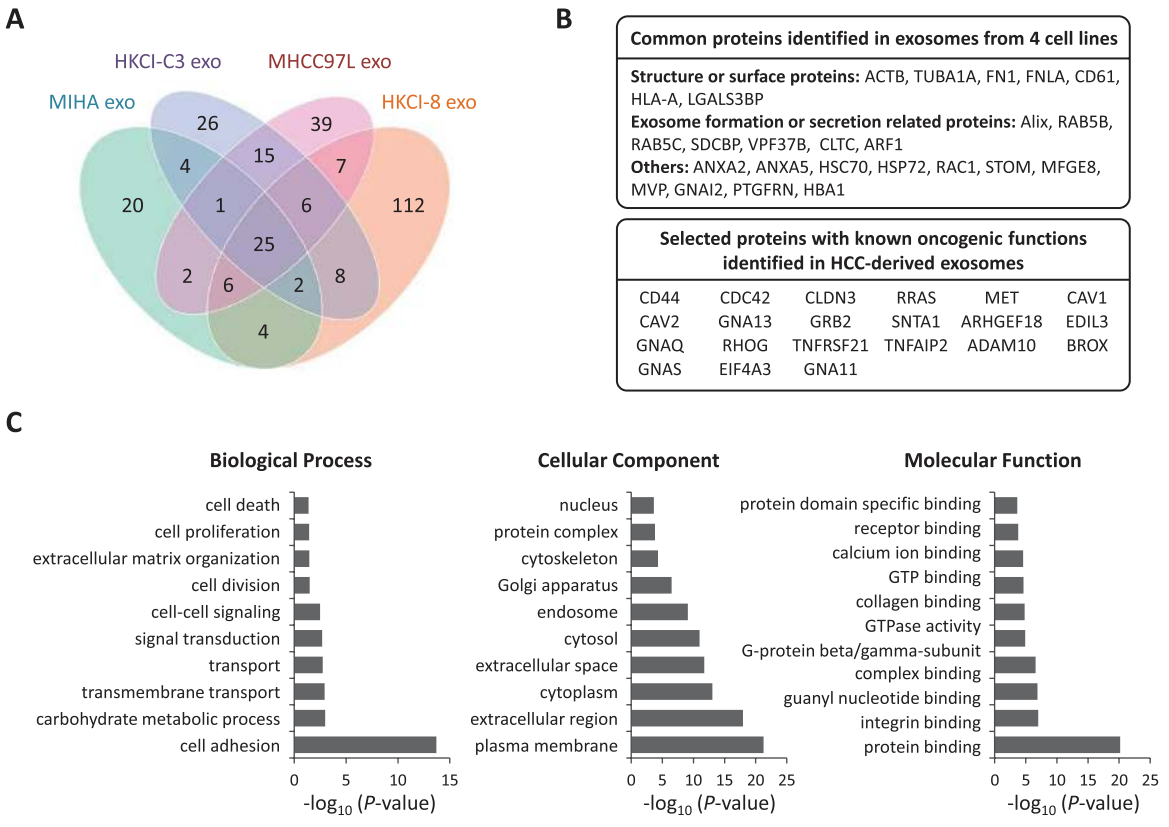

Figure 3. Mass spectrometry analysis for exosomal proteins. (**A**) Venn diagram comparison of exosomal proteomes of an immortalized hepatocyte and three HCC cell lines. (**B**) Exosomal proteins shared in four cell lines (left), or selected proteins with known oncogenic functions identified in HCC-derived exosomes (right) were listed, respectively. (**C**) GO enrichment analysis of exosomal proteins specific in three HCC cell lines. The top 10 significantly enriched GO categories under biological process, cellular component and molecular function were indicated.

lines but not MIHA, which might reflect cancer-related features (Supplementary Figure 3A, available at *Carcinogenesis* Online). Besides, Venn diagram of their exosomal protein profiles also indicated each cell lines had different protein constitution, as large amount of proteins were only detected in a single cell line's exosomes (Figure 3A).

To further characterize related pathways underlying those shuttled exosomal proteins, we performed GO enrichment analysis of 213 HCC specific proteins (Figure 3C). Results showed that the biological process 'cell adhesion' was significantly enriched in HCC exosomes, with the majority of exosomal proteins localized in plasma membrane, extracellular regions and cytoplasm. GO molecular function also suggested these exosomal proteins were markedly enriched for 'protein binding' and 'integrin binding'.

Motile HCC-derived exosomes induces migration and invasion of non-motile MIHA cells

Because exosomes from motile HCC cell lines showed high amount of tumorigenic RNAs and proteins, we next investigated whether they could affect the migratory and invasive properties of normal hepatocyte. Functional studies showed exosomes from highly metastatic HCC cell lines MHCC97L and HKCI-8 could significantly enhance MIHA cells migration (MHCC97L: $P = 0.0003$, HKCI-8: $P = 0.0049$) and invasion (MHCC97L: $P = 0.0198$; HKCI-8: $P = 0.0128$) (Figure 4Aand B). However, exosomes from non-motile HCC cell line HKCI-C3 had negligible effect on MIHA motility (migration: $P = 0.1490$; invasion: $P = 0.3551$) (Figure 4C).

To explore what caused the differential inducing effects of HCC exosomes on MIHA cell motility, we selected coding genes that were highly expressed in exosomes derived from MHCC97L, then HKCI-8, but absent in MIHA and HKCI-C3 for validation (Supplementary Table 5, available at *Carcinogenesis* Online). Interestingly, we found three S100 proteins, S100A4, S100A10 and S100A11, were among the top ranked candidates. Previous studies have suggested that members of S100 protein family, especially S100A4, played a role in the regulation of cell motility and invasiveness of metastatic cells via modulating the cytoskeleton dynamics (15). Quantitative PCR confirmed S100A4 to be uniquely expressed in MHCC97L and HKCI-8 cells and their exosomes (Figure 4D). RNA-sequencing also identified two caveolins, CAV1 and CAV2, with highest expressions in MHCC97L exosomes, which were verified by real-time PCR (Figure 4D).

In examining the exosomal proteins, given that MHCC97L exosomes exerted the most significant effect on MIHA motility (Figure 4A), we hence focused our analysis on distinct proteins expressed in MHCC97L exosomes. The hepatocyte growth factor (HGF)-MET signaling was demonstrated to have crucial roles in controlling cell proliferation, migration and invasion (16). Previous study reported melanoma exosomes could horizontally transfer exosomal MET to bone marrow progenitors to support tumor growth and metastasis (12). Consistent with these reports, we also detected MET protein in MHCC97L exosomes from mass spectrometry (Supplementary Figure 3B, available at *Carcinogenesis* Online). Western blot confirmed the levels of MET and p-MET were higher in both MHCC97L and HKCI-8 cell lines and secreted exosomes compared to MIHA and HKCI-C3 cells and their exosomes, respectively (Figure 4E). Moreover, CAV1, CAV2 and S100A4, whose mRNA transcripts were carried inside

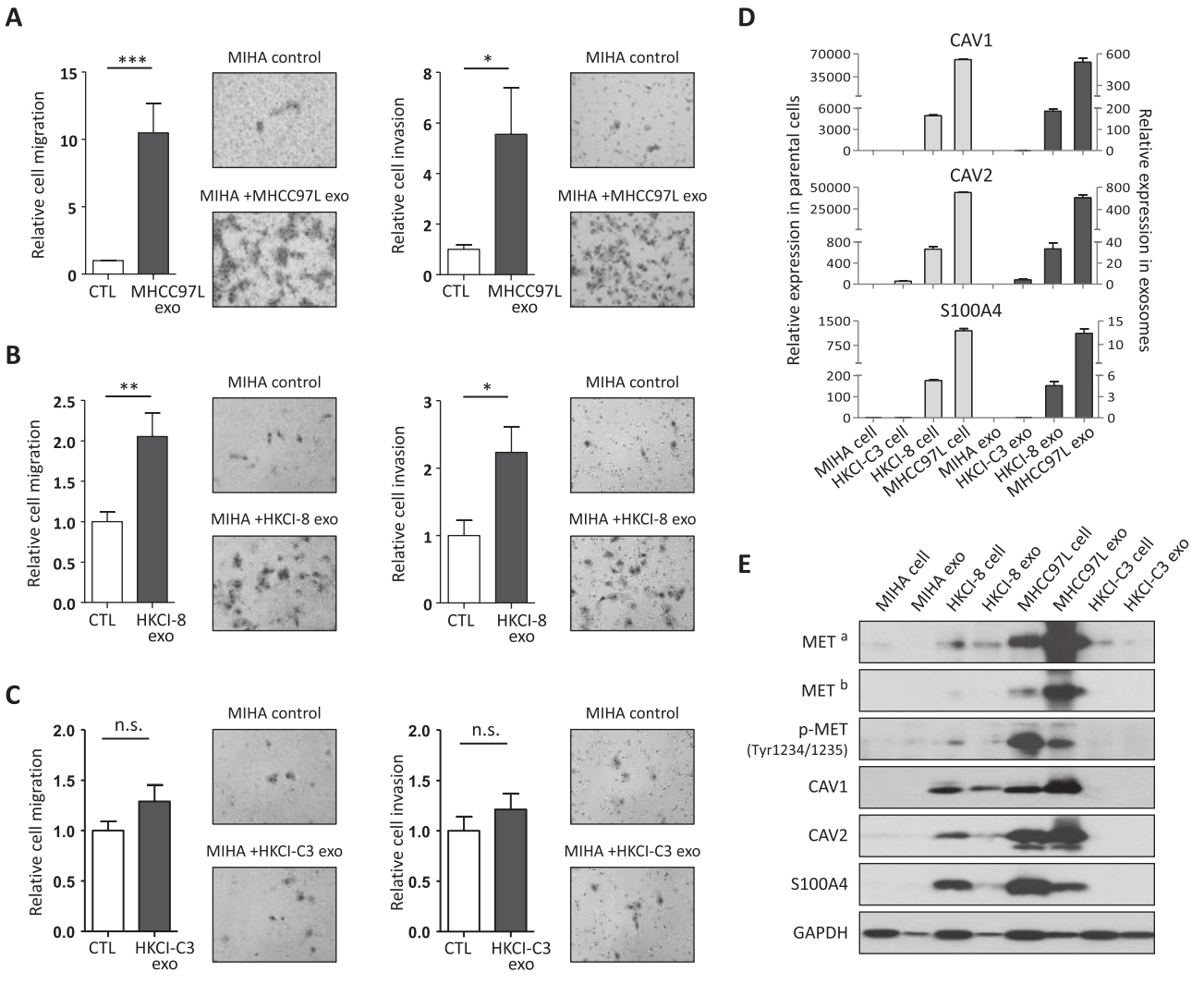

Figure 4. Motile HCC-derived exosomes induces migration and invasion of non-motile MIHA. Functional effects of MHCC97L (**A**), HKCI-8 (**B**) and HKCI-C3 (**C**) derived exosomes on MIHA cell migratory and invasive abilities. Each assay was treated with 10 μg purified exosomes. Data shown represent mean ± SEM from three independent experiments (Student's *t*-test; $^{*}P < 0.05$, $^{**}P < 0.01$, $^{***}P < 0.001$, n.s. no significance). (**D**) Relative expression levels of CAV1, CAV2 and S100A4 in parental cell lines and their corresponding exosomes by quantitative PCR. Data were normalized by RNA amount. (**E**) Representative western blot of MET, p-MET (Tyr1234/1235), CAV1, CAV2, S100A4 and GAPDH in exosomes and their originated cells. MET^{a}: high exposure; MET^{b}: low exposure.

the exosomes, also showed high content of these proteins in MHCC97L and HKCI-8 exosomes (Figure 4E).

Uptake of MHCC97L-derived exosomes triggers a signaling network in favor of motility in MIHA cells

To further define the potential mechanisms underlying the MHCC97L exosomes-induced MIHA motility, we analyzed the expression levels of candidate genes in MIHA cells after treatment with MHCC97L exosomes. After 15 h incubation, CAV1, CAV2 and S100A4 mRNA levels were significantly increased in MHCC97L exosomes-treated MIHA cells as shown by quantitative PCR (CAV1: $P = 0.0042$; CAV2: $P < 0.0001$; S100A4: $P = 0.0006$) (Figure 5A). In addition, increased protein levels of MET, CAV1 and CAV2 were also observed in MIHA after the treatment with MHCC97L exosome, suggesting the horizontal transfer of exosomal molecules from MHCC97L to MIHA by exosomes (Figure 5B). However, S100A4 protein level was only slightly increased after exposure to MHCC97L exosomes (Figure 5B). One possible reason for this could be a high endogenous level of S100A4 in MIHA masked the slight increase from the shuttled S100A4 mRNA or protein.

Since both mRNA and protein of CAV1 and CAV2 were present in MHCC97L-derived exosomes (Figure 4Dand E) and previous studies have shown that exosomal mRNA could be translated into protein in recipient cells (7,8), we next investigated if the increased protein level of CAV1 and CAV2 in MIHA was due to translation of exogenous mRNA. To differentiate the source of CAV1, we pretreated MIHA with siRNAs against CAV1 or CAV2 before MHCC97L exosomes incubation. Pretreatment of siCAV1 did not reduce CAV1 level in MIHA, indicating that the majority of increased CAV1 was from the horizontal transfer of exosomal protein (Figure 5Ci). Similar result was also obtained in siCAV2 pretreated MIHA (Figure 5Cii)

Previous studies showed HCC patients with aberrant activation of HGF/c-Met signaling pathway have poorer prognosis and more aggressive phenotype (17). Deregulated c-MET triggers multiple downstream signaling pathways, such as PI3K pathway (PI3K-AKT-mTOR) and MAPK signaling pathway (RAS-RAF-MEK-ERK) (16). Similarly, CAV1 has been shown to be highly expressed in metastatic HCC tumors and its increased expression associated with HCC tumorigenesis and metastasis (18).

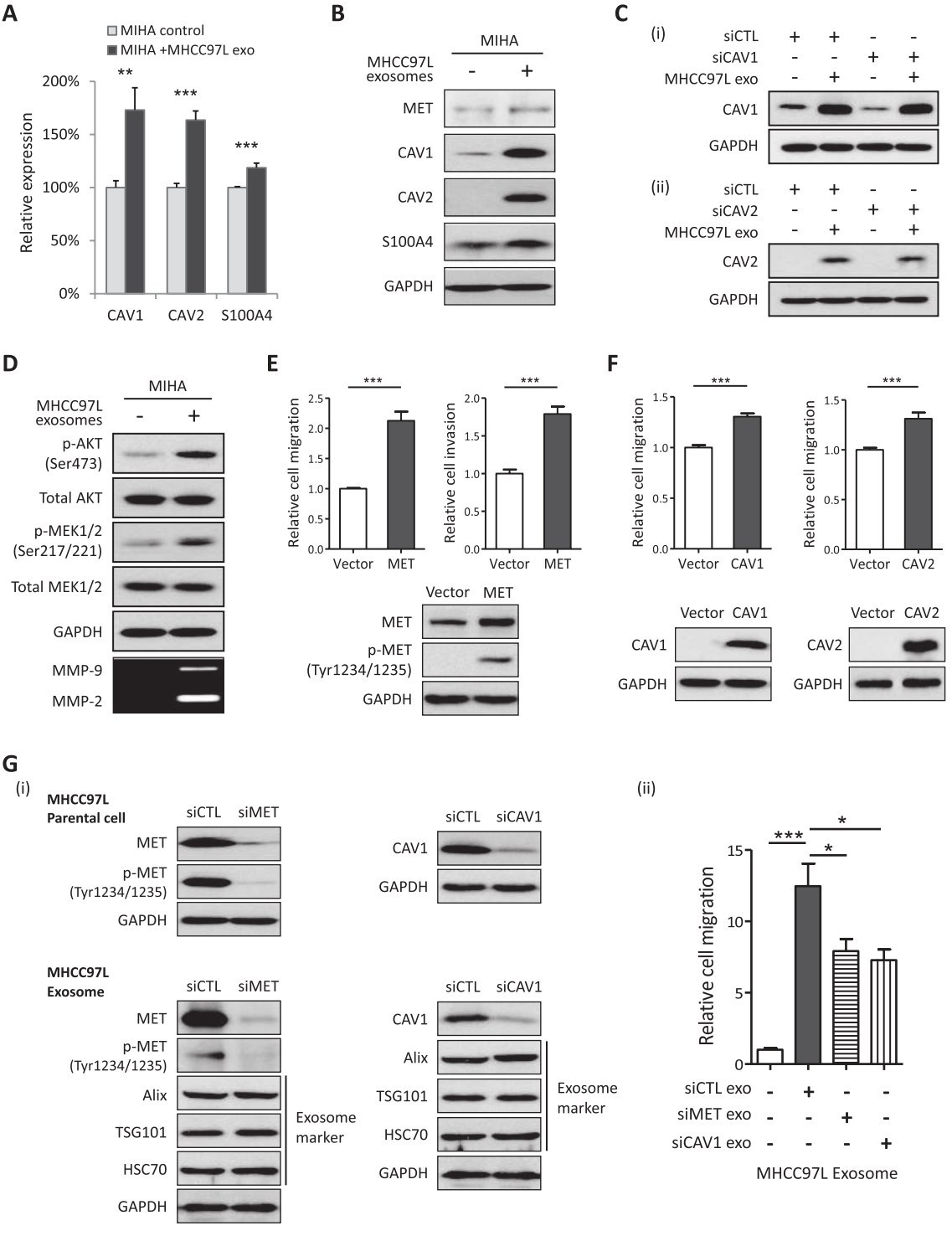

Figure 5. Uptake of MHCC97L-derived exosomes triggers a signaling network in favor of MIHA cell motility. (**A**) Quantitative real-time PCR analysis of CAV1, CAV2 and S100A4 in MIHA with or without MHCC97L-derived exosomes exposure. The mean value was expressed as a percentage relative to MIHA cells in absence of exosomes treatment. (**B**) Immunoblotting analysis of MET, CAV1, CAV2 and S100A4 of MIHA cells in presence or absence of MHCC97L exosomes incubation. (**C**) CAV1 (i) and CAV2 (ii) protein levels of MHCC97L exosomes-treated MIHA cells in the presence or absence of siRNA pretreatment. (**D**) Western blot analysis of total AKT, p-AKT (Ser473), total MEK1/2 and p-MEK1/2 (Ser217/221) in MIHA cells treated with purified MHCC97L exosomes. Secreted MMP-2 and MMP-9 activities were measured by gelatin zymography. GAPDH was used as a loading control. (**E**) Overexpression of MET increased MIHA cell migratory and invasive abilities (migration: $P < 0.0001$, invasion: $P < 0.0001$). (**F**) Ectopic expression of CAV1 and CAV2 conferred increased cell migration of MIHA (CAV1: $P < 0.0001$, CAV2: $P = 0.0004$). (**G**) (i) Knockdown efficiency of MET and CAV1 in MHCC97L parental cells and their derived exosomes was assessed by Western blot. (ii) Depletion of MET and CAV1 in MHCC97L could abrogate the effect of MHCC97L exosomes-induced MIHA migration (siMET: $P = 0.0236$, siCAV1: $P = 0.0143$). Data shown represent mean ± SEM from three independent experiments (Student's *t*-test; $^{*}P < 0.05$, $^{**}P < 0.01$, $^{***}P < 0.001$).

Moreover, increased AKT and ERK activities have been shown to be under the modulation of CAV1-mediated motility (19,20). To determine whether the signaling pathways of these shuttled molecules could be activated in MIHA, we analyzed the phosphorylation levels of downstream effectors of MET and CAV1 signaling, such as p-AKT and p-MEK. Western blot confirmed

AKT and MEK1/2 phosphorylation was significantly increased in MIHA after exposure to MHCC97L exosomes (Figure 5D). We also found MMP-2 and MMP-9 to be markedly increased in the conditioned medium of MIHA cells after MHCC97L exosomes treatment (Figure 5D).

To further assure the roles of MET and caveolins in the MHCC97L-induced MIHA motility, we overexpressed MET, CAV1 and CAV2 in MIHA. Functional investigation confirmed that overexpression of MET could significantly enhance MIHA cell migratory and invasive abilities (migration: $P < 0.0001$, invasion: $P < 0.0001$) (Figure 5E), whilst ectopic expression of CAV1 and CAV2 conferred increased cell migration of MIHA (CAV1: $P < 0.0001$, CAV2: $P = 0.0004$) (Figure 5F). To affirm a direct role for MET and CAV1 in the induction of MIHA motility, knockdown of MET and CAV1 in MHCC97L parental cell was carried out to deplete RNA and protein of these two genes in exosomes prior to re-transfection into MIHA. Following siRNA knockdown, a corresponding decrease in the protein level of MET and CAV1 was shown in derived exosomes (Figure 5Gi). Indeed, depletion of MET and CAV1 could significantly abrogate the effect of MHCC97L exosomes induced MIHA cell migration (siMET: $P = 0.0236$, siCAV1: $P = 0.0143$) (Figure 5Gii). However, residual migratory activity could still be detected suggesting that other exosomal RNAs/proteins are probably involved in the exosome-mediated hepatocyte motility.

Taken together, we hypothesize that motile HCC could secrete stimulatory exosomes carrying RNAs and proteins, including MET proto-oncogene, caveolins and S100 family. After internalized by hepatocytes, exosomes were able to induce MIHA cells to migratory and invasive abilities by activating PI3K/AKT and MAPK signaling pathways. Activated hepatocytes increased the secretion of MMP-2 and MMP-9 into the exterior, which might in turn facilitate protrusive activity of tumor cells. A schematic diagram of our postulation is shown in Figure 6.

Discussion

Cancer development relies on the interactions between cancer cells and different components of its microenvironment. Recent studies have indicated cancer cell secreted exosomes played an important role in cell–cell communication by conveying information between tumor cells and between tumor and neighboring cells, such as in HCC (21). However, the molecular changes induced between hepatoma cells and the main cell type of the liver, hepatocyte, remain largely unknown. Here, we provide evidence that metastatic HCC cell lines could prompt migratory and invasive abilities of immortalized hepatocyte by the horizontal transfer of molecules via exosomes. On the contrary, exosomes from HCC cells with low metastatic capacity have no significant effect on MIHA cells motility, suggesting exosomes function depends on their content and the property of parental cell. Notably, exosomes derived from highly malignant HCC cells carried a variety of oncogenic mRNAs and proteins, such as MET proto-oncogene, caveolins and S100 family members. Internalized of these shuttled molecules by immortalized hepatocytes could trigger multiple signaling pathways that led to enhanced secretion of matrix degrading proteases, MMP-2 and MMP-9. It is plausible that tumor-activated hepatocyte might act as leading cells that moved in the front, while cancer cells could invade through the tract generated by leading cells (22). Thus, HCC tumor cells could modify normal hepatocytes in their environment to facilitate tumor growth, invasion and metastases via exosomes.

In this study, we identified the level of MET protein to be extremely high in motile MHCC97L cells and significantly enriched in their exosomes, which might be the principle mediator of exosomes-mediated hepatocyte motility (Figure 4E). Aberrantly activated MET signaling plays a pivotal role in tumor growth, angiogenesis and metastasis (16). While we found MET to be markedly enriched in MHCC97L exosomes, the mechanism by which MET was selectively packaged into exosomes remained unknown. The juxtamembrane region of MET contains a docking site, Y1003, which can be ubiquitinated by E3 ubiquitin ligase Cbl (23). Since ubiquitin-dependent endosomal sorting machinery has been defined recently (24), one possible mechanism is that ubiquitinated MET could be endocytosed, transported to the endosomal compartment, packaged into exosomes and, finally, released into the extracellular environment.

S100A4, CAV1 and CAV2 were also significantly enriched in metastatic HCC-derived exosomes, both in mRNA and protein

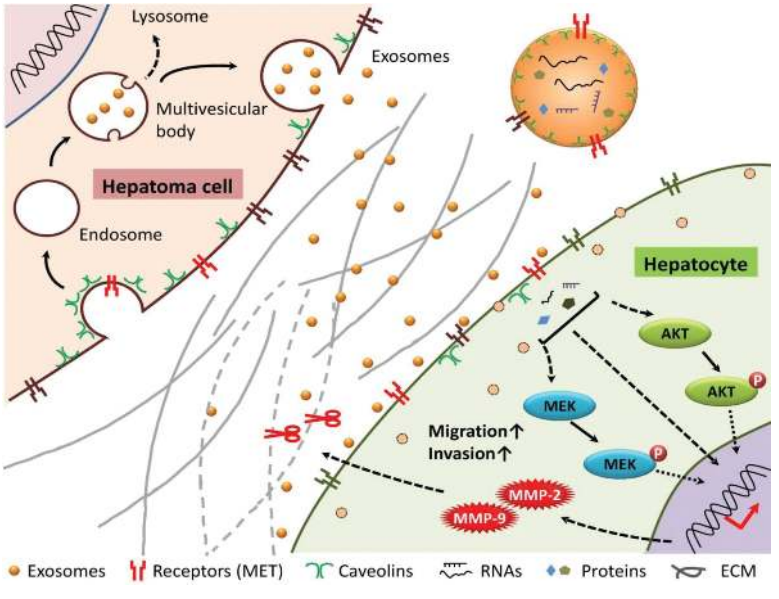

Figure 6. A schematic model of the interplay between heptatoma cells and hepatocytes in tumor invasion.

forms (Figure 4Dand E). S100A4, a member of the S100 family of calcium-binding proteins, has been shown to play a role in tumor progression and metastasis (25). Although S100A4 is a protein without any known signal peptide for secretion, it has been reported to be detectable in extracellular space (26). Here, we provide a new mechanism for its occurrence outside of cancer cells, where S100A4 could be secreted into extracellular microenvironment via tumor exosomes (Figure 4E). Both intracellular and extracellular S100A4 were demonstrated to accelerate tumor invasive growth through the transcriptional regulation of MMPs (27,28). Caveolae, a special type of lipid raft, are small invaginations of the plasma membrane in many cell types. It has been shown that target molecules can be internalized from the lipid rafts by caveolae-mediated endocytosis and shuttled to the early endosomes, which would later undergo exosomes formation and secretion process (29). Moreover, overexpression of CAV1 has been shown in metastatic HCC tumors (18,30), and exosomes secreted by metastatic melanoma cells (31). In line with their findings, we observed that higher caveolins expressions correlated with motile HCC cell lines (Figures 1A, 4D and E).

In summary, we describe a comprehensive RNA and protein profiling of exosomes derived from motile and non-motile HCC cell lines. We found novel interaction between HCC tumor cells and immortalized hepatocyte via exosomes. Our study also identified multiple oncogenic molecules carried in tumor-derived exosomes that might be responsible for exosomes-induced hepatocyte migration and invasion. Our proteome analysis also suggested proteins that might be associated with exosomes formation. Among them, syndecan–syntenin–ALIX is known to support biogenesis of exosomes and the segregation of signaling cargo to these vesicles (32). Rab GTPase family members, which are capable to manipulate different steps of the exosomes secretion pathway, were identified (33). We also found several components of endosomal protein sorting complex, such as VPS28 and VPS37, whose functions are required for exosome cargo sorting process (24). Our data hence supports, in addition to promoting cancer progression, necessary proteins for biogenesis and secretion are also present in exosomes.

Supplementary material

Supplementary Table 1–5 and Figures 1–3 can be found at http://carcin.oxfordjournals.org/

Funding

Collaborative Research Fund from the Hong Kong Research Grants Council (CUHK8/CRF/11R).
Conflict of Interest Statement: None declared.

References

1. Tang, Z.Y. et al. (2004) A decade's studies on metastasis of hepatocellular carcinoma. J. Cancer Res. Clin. Oncol., 130, 187–196.
2. Li, Y. et al. (2012) Hepatocellular carcinoma: insight from animal models. Nat. Rev. Gastroenterol. Hepatol., 9, 32–43.
3. Wu, S.D. et al. (2012) Role of the microenvironment in hepatocellular carcinoma development and progression. Cancer Treat. Rev., 38, 218–225.
4. Budhu, A. et al. (2006) Prediction of venous metastases, recurrence, and prognosis in hepatocellular carcinoma based on a unique immune response signature of the liver microenvironment. Cancer Cell, 10, 99–111.
5. Vidal-Vanaclocha, F. (2011) The liver prometastatic reaction of cancer patients: implications for microenvironment-dependent colon cancer gene regulation. Cancer Microenviron., 4, 163–180.
6. Théry, C. et al. (2002) Exosomes: composition, biogenesis and function. Nat. Rev. Immunol., 2, 569–579.
7. Skog, J. et al. (2008) Glioblastoma microvesicles transport RNA and proteins that promote tumour growth and provide diagnostic biomarkers. Nat. Cell Biol., 10, 1470–1476.
8. Valadi, H. et al. (2007) Exosome-mediated transfer of mRNAs and microRNAs is a novel mechanism of genetic exchange between cells. Nat. Cell Biol., 9, 654–659.
9. Atay, S. et al. (2014) Oncogenic KIT-containing exosomes increase gastrointestinal stromal tumor cell invasion. Proc. Natl. Acad. Sci. USA, 111, 711–716.
10. Luga, V. et al. (2012) Exosomes mediate stromal mobilization of autocrine Wnt-PCP signaling in breast cancer cell migration. Cell, 151, 1542–1556.
11. Wong, N. et al. (2005) Transcriptional profiling identifies gene expression changes associated with IFN-alpha tolerance in hepatitis C-related hepatocellular carcinoma cells. Clin. Cancer Res., 11, 1319–1326.
12. Peinado, H. et al. (2012) Melanoma exosomes educate bone marrow progenitor cells toward a pro-metastatic phenotype through MET. Nat. Med., 18, 883–891.
13. Poon, T.C. et al. (2012) Proteomic analysis reveals platelet factor 4 and beta-thromboglobulin as prognostic markers in severe acute respiratory syndrome. Electrophoresis, 33, 1894–1900.
14. Jiao, X. et al. (2012) DAVID-WS: a stateful web service to facilitate gene/protein list analysis. Bioinformatics, 28, 1805–1806.
15. Kriajevska, M. et al. (1998) Metastasis-associated Mts1 (S100A4) protein modulates protein kinase C phosphorylation of the heavy chain of nonmuscle myosin. J. Biol. Chem., 273, 9852–9856.
16. Birchmeier, C. et al. (2003) Met, metastasis, motility and more. Nat. Rev. Mol. Cell Biol., 4, 915–925.
17. Kaposi-Novak, P. et al. (2006) Met-regulated expression signature defines a subset of human hepatocellular carcinomas with poor prognosis and aggressive phenotype. J. Clin. Invest., 116, 1582–1595.
18. Tse, E.Y. et al. (2012) Caveolin-1 overexpression is associated with hepatocellular carcinoma tumourigenesis and metastasis. J. Pathol., 226, 645–653.
19. Li, L. et al. (2003) Caveolin-1 maintains activated Akt in prostate cancer cells through scaffolding domain binding site interactions with and inhibition of serine/threonine protein phosphatases PP1 and PP2A. Mol. Cell. Biol., 23, 9389–9404.
20. Park, J.H. et al. (2009) Caveolin-1 plays important role in EGF-induced migration and proliferation of mouse embryonic stem cells: involvement of PI3K/Akt and ERK. Am. J. Physiol. Cell Physiol., 297, C935–C944.
21. Lemoinne, S. et al. (2014) The emerging roles of microvesicles in liver diseases. Nat. Rev. Gastroenterol. Hepatol., 11, 350–361.
22. Gaggioli, C. et al. (2007) Fibroblast-led collective invasion of carcinoma cells with differing roles for RhoGTPases in leading and following cells. Nat. Cell Biol., 9, 1392–1400.
23. Jeffers, M. et al. (1997) Degradation of the Met tyrosine kinase receptor by the ubiquitin-proteasome pathway. Mol. Cell. Biol., 17, 799–808.
24. Katzmann, D.J. et al. (2001) Ubiquitin-dependent sorting into the multivesicular body pathway requires the function of a conserved endosomal protein sorting complex, ESCRT-I. Cell, 106, 145–155.
25. Mishra, S.K. et al. (2012) S100A4 calcium-binding protein is key player in tumor progression and metastasis: preclinical and clinical evidence. Cancer Metastasis Rev., 31, 163–172.
26. Chaabane C. et al. (2014) Extracellular S100A4 induces smooth muscle cell phenotypic transition mediated by RAGE. Biochim. Biophys. Acta, in press.
27. Saleem, M. et al. (2006) S100A4 accelerates tumorigenesis and invasion of human prostate cancer through the transcriptional regulation of matrix metalloproteinase 9. Proc. Natl. Acad. Sci. USA, 103, 14825–14830.
28. Schmidt-Hansen, B. et al. (2004) Extracellular S100A4(mts1) stimulates invasive growth of mouse endothelial cells and modulates MMP-13 matrix metalloproteinase activity. Oncogene, 23, 5487–5495.
29. Valapala, M. et al. (2011) Lipid raft endocytosis and exosomal transport facilitate extracellular trafficking of annexin A2. J. Biol. Chem., 286, 30911–30925.

30. Cokakli, M. et al. (2009) Differential expression of Caveolin-1 in hepatocellular carcinoma: correlation with differentiation state, motility and invasion. BMC Cancer, 9, 65.
31. Logozzi, M. et al. (2009) High levels of exosomes expressing CD63 and caveolin-1 in plasma of melanoma patients. PLoS One, 4, e5219.
32. Baietti, M.F. et al. (2012) Syndecan-syntenin-ALIX regulates the biogenesis of exosomes. Nat. Cell Biol., 14, 677–685.
33. Ostrowski, M. et al. (2010) Rab27a and Rab27b control different steps of the exosome secretion pathway. Nat. Cell Biol., 12, 19–30.